Iranian (Iranica) Journal of Energy & Environment
Journal Homepage: www.ijee.net
IJEE an official peer review journal of Babol Noshirvani University of Technology, ISSN:2079-2115

Bubble Dynamics and Nucleate Pool Boiling of Natural Convection

S. Bagheri[1], S. A. A. Oloomi*[1], S. A. A. Mirjalily[1], A. Zare-Shahabadi[2]

[1] *Department of Mechanical Engineering, Yazd Branch, Islamic Azad University, Yazd, Iran*
[2] *Department of Mechanical Engineering, Technical and Vocational University (TVU), Tehran, Iran*

P A P E R I N F O

Paper history:
Received 08 June 2022
Accepted in revised form 26 July 2022

Keywords:
Bubble diameter
Bubble production frequency
Nuclear boiling
Volume fraction

A B S T R A C T

The phenomenon of nuclear boiling has always been recognized suitable for heat transfer between different boiling regimes. Study on boiling is considered as a new field which meets different research and industrial needs such as heat transfer in nuclear reactors, cooling units, rocket motors, electronic equipment cooling, batteries, etc. In this study, a chamber with immiscible fluid, water, steam, and air, having a side wall with uniform heat flux has been studied in 3D. To do so, we first considered the prediction of the heat flux interval for which the boiling occurs in the form of nuclear boiling. In this study, two-phase fluid volume (VOF) approach was used for modelling boiling on the vertical wall and two-phase flow. In this research, Ansys software package was used for numerical modelling and numerical simulation. Distribution of the velocity field follows more uniform pattern in dimensionless heights less than 0.9. In this study, bubbles are only present near a wall with heat flux that has a lower Rayleigh number. Also, existence of these bubbles on the wall, which prevents fluid infiltration, affects vortices caused by natural convection. However, the general and uniform patterns of vortices remain unchanged in most part of the fluid, which is because of the limited amount of bubbles near the wall with heat flux. Natural convection increases the height of fluid inside the chamber, which leads to the formation of stronger vortices at a dimensionless height of 0.9 that has a high Raleigh number due to high heat flux. In this case, the continuous use of heat flux gives rise to the production of bubbles over time.

***doi**: 10.5829/ijee.2022.13.04. 08*

NOMENCLATURE

h	Convection coefficient ($W.m^{-2}K^{-1}$)	u,v	Velocity vector at x,y ($m.s^{-1}$)
C_p	Specific heat at constant pressure ($J.kg^{-1}K^{-1}$)	**Subscripts**	
k	Conduction coefficient ($W.m^{-1}K^{-1}$)	g	Gas phase
h_{fg}	Latent heat of vaporization ($J.kg^{-1}$)	*v*	Vapor phase
L	Length of chamber (m)	sat	Saturation
W	Width of chamber (m)	**Greek Symbols**	
Ra	Rayleigh number	ρ	Density (kgm^{-3})
S	Source term ($kg.m^{-3}s^{-1}$)	μ	Dynamic viscosity (Pa.s)
T	Temperature (K)	α	Thermal diffusion coefficient (m^2s^{-1})

INTRODUCTION

Study on boiling is considered as a new field which means different research and industrial needs such as heat transfer in nuclear reactors, cooling units, rocket motors, electronic equipment cooling, batteries, etc. Owing to phase change, heat in boiling is transferred from the hot surfaces in the form of bubble production. Because of the strong dependence of bubble production rate and heat transfer, on understanding the production phenomenon, bubble growth and separation from the surface would be essential. The growth and separation of bubbles from the

*Corresponding Author Email: amiroloomi@iauyazd.ac.ir (S. A. A. Oloomi)

Please cite this article as: S. Bagheri, S. A. A. Oloomi, S. A. A. Mirjalily, A. Zare-Shahabadi, 2022. Bubble Dynamics and Nucleate Pool Boiling of Natural Convection, Iranian (Iranica) Journal of Energy and Environment, 13(4), pp.384-397. Doi: 10.5829/ijee.2022.13.04.08

surface is done under the influence of various forces as to surface tension and buoyancy force. In the early stages of bubble formation, tensile forces predominate over buoyancy, as the size of the bubble increases the amount of buoyancy force exceeds the surface tensile force; therefore, the bubble is separated from the hot surface. In fact, investigating the rate of bubble formation, bubble growth, its separation from the surface, and also the rate of heat transfer would entail sufficient knowledge of the bubble dynamics. Bubble dynamics include parameters such as the distribution of active bubble sites, bubble diameter, bubble reactivation time, bubble growth time, etc., in the current study, we have numerically investigated the mentioned parameters and the effect of natural convection on this phenomenon. Jakob [1] has presented the first report on the relationship between wall heat flux, and the density of active nuclear boiling sites. His observations merely included surfaces with relatively low heat flux. Hsu and Graham [2] made observations on different studies regarding the relationship among heat flux or heat transfer coefficient, wall temperature difference and density of active bubble sites. Lee and Nydah [3] numerically studied the growth of the bubble from the early stage of formation, to its final separating from the surface; They discovered that at the time of detachment, bubble movement in a general sense causes forced heat transfer near the surface, which itself speeds up heat transfer; furthermore, a study on the thin layer of fluid which is formed after the bubble is detached from the surface, has a great effect on bubble growth and heat transfer. Regarding the shape of the upper part of the bubble, significant changes could be observed during its growth. Welch [4] studied bubble growth via a straightforward numerical method; owing to the existence of a temperature profile of two phases, He used a moving mesh for investigating the computations accuracy**.** Lay and Dhir [5] carried out a comprehensive study on the thin fluid layer and its consideration. They could predict the diameter of bubble root in a well-developed boiling heat transfer mode [5]. Son et al. [6] conducted a numerical study of a bubble's dynamics and heat transfer in horizontal plate boiling. In this study, what is accurately considered is the effect of the bubble contact angle on the surface and also the temperature of the wall superheat; to consider near-surface fluid micro-layers, the geometry is divided into two micro and macro zones. The lubrication theory has been applied to the laws governing the micro area either. The results of this study have shown that with the bubble contact angle with the surface, and the surface temperature of the wall, the diameter of bubbles separated from the surface increases [6]. In another study, using the Level set method, the two-phase contact surface in boiling was investigated. In this study, the effect of the bubbles on the heat transfer, the shape of the flow near the wall, and heat transfer in a fluid microwave on the surface were numerically studied [7]. To investigate the three-dimensional state of the bubble fusion of two or three adjacent holes, Mukherjee and Dhir [8] used level set method. Using the Level Contour Reconstruction Method, Shin et al. [9] investigated the three-dimensional numerical evaluation of nuclear boiling. In their study, they focused on the effect of the number and density of cavities of the surface in a numerical model by varying the surface area of the cavity. The Nusselt number results were in accordance with the experimental studies, which stipulated the prominence of the neighboring holes' influence on the surface; though, owing to the three-dimensional geometry, in their studies done on simplification, the effects of fluid microlayers were discussed [9]. Using the free mesh method (MPS-MAFL), Yoon et al. [10] conducted a direct numerical study on detachment, bubble growth, and fluid uptake in nuclear boiling. In this study, the coupled energy relationship with the bubble motion equation has been contemplated; besides, the heat transfer mechanism has been investigated [10]. Son and Dir [11] numerically studied the boiling of the horizontal plane with high heat fluxes. Due to the importance of fluid microlayers, special grouting has been used in this area. Here in this study, water is considered as a fluid having constant properties in either the use phase or the type of flow. Different effective factors including the wall superheat temperature, the number and density of cavities on the surface, the time required for reactivating the cavities to produce subsequent bubbles, etc. have been precisely considered. The results of this study have shown that as the number of surface active cavities increases, the heat flux increases either. The increase of the wall superheat temperature would get to the quick formation of bubble columns, and a decrease in the nuclei activation time, which increase the heat transfer coefficient to a great extent [11]. Chou and Yu [12] studied the influence of the superheated wall temperature, total size and size of the pits, and also the influence of fluid properties on the heat transfer of nuclear boiling. McHale et al. [13] experimentally and numerically with different roughness's investigated the nuclear boiling of surfaces; apart from that, they reported their direct effect on the bubbles shape and their detachment from the surface. The vertical interconnection in the nuclear boiling of an artificial cavity was studied experimentally by Hutter et al. [14]. They observed that as pressure decreases and surface superheat temperature increases, the interconnectivity increases as well either. Sanna et al. [15] studied the nuclear boiling of surfaces of different genders numerically; They studied the effect of the position and number of surface cavities on the time needed for activating the cavities, growth time, etc. The results of this study for surfaces made of titanium and silicon, under the same conditions, indicated that the surfaces with titanium cores, being compared to the surfaces with silicon cores, were more active; apart from that, in comparison to the silicon surface, the titanium surface cavities behaved more independently [15]. Jung

and Kim [16] studied and measured bubble dynamics and heat transfer in a nuclear bubble from a horizontal plane experimentally. They observed that heat transfer was deeply correlated with surface fluid microlayers [16]. Kunkelmann and Stephan [17] in the presence of HFE-7100 refrigerant and bubble shape, studied numerically the transient boiling heat transfer during growth and detachment. Jia et al. [18] investigated the experimental and numerical study of surface-to-surface nuclear boiling. They observed the same bubble shape in both the experimental and numerical studies; however, being compared to the experimental one, in the numerical study the separation time was longer. The results of this study indicated that the vapor phase temperature was distributed near the hot wall with homogeneous circles [18]. Using VOSET, Ling et al. [19] studied the two-dimensional nuclear boiling method numerically; to investigate bubble dynamics in the presence of nuclear boiling convection, they performed direct numerical simulations. The relationship between bubble growth and heat flux was investigated in the relatively low Reynolds number; later they observed that the shape of the bubble during formation and growing was similar to the results of experimental studies; however, there were differences after its departure from the surface [20]. Utaka et al. [21] measured and studied microlayers of water and ethanol fluids in horizontal boiling of nuclear. The results of this study showed that although the microlayer was similar to ethanol, water was twice thicker than that (ethanol). Different studies have been conducted for investigating the effect of surface positioning angle on nuclear boiling. Marcus and Dropkin [22] studied the shape of the plate on the heat transfer of nuclear boiling experimentally; during this procedure they observed the specific effect of plate angle on heat transfer. Moreover, Sarker et al. [23] studied the dynamics of a bubble during the infrared nuclear boiling of a vertical heater surface so as to investigate the influence of surface properties such as wetness and roughness experimentally. The results of this study are indicating of the huge impact of surface roughness on bubble growth and detachment which is arising from the effect that surface has on the fluid microlayer formed below the bubbles. Salari et al. [24] studied the effect of the static bubbles on the levels of lead-acid battery electrodes, and on natural convection currents. They investigated the effect of Rayleigh number and bubble parameters on fluid flow structure, heat flux, velocity distribution, temperature, mean Nusselt number, etc. The results of this study have indicated that owing to the effect of bubble insulation on the wall and as a result, increasing the surface temperature of the electrodes, as the number of bubbles increases, conversely the average Nusselt number decreases. The presence of bubbles also causes the deviation of the field from the flow field [24].

The numerical methodology and developed modelling disclosed that the combined application of the basic deterministic conservation laws for the continuous two-phase flow field, and the stochastic characteristics of the vapor generation at the heated wall might simulate complex pool boiling conditions [25, 26]. The major roles of nanoparticles affected by nanofluid boiling heat transfer, including the bulk effect associated with suspended nanoparticles of the fluid and their thermal properties (thermal conductivity, viscosity, heat capacity and density), shall be well understood; the surface effect associated with deposit nanoparticles, which have modified the characteristics of heating surface (wettability, homogeneity, roughness and solid surface tension, etc.; would be achieved by careful experimental observations and numerical simulations. For find suitable nanofluids for different engineering systems more effort is required; from this perspective, testing more types of nanoparticles is needed [27].

PROBLEM STATEMENT AND GEOMETRIC MODELING

Three-dimensional geometry of the present study and their boundary conditions are shown in Figure 1. The side wall has a uniform heat flux that is corresponding to the height of the area with the fluid height inside the chamber. The compartment is filled with immiscible fluids, steam, water, and air. The other walls of chamber are adiabatic; The upper part of the chamber has a Pressure outlet boundary condition. The initial set temperature is 373.15K for water and steam, and is 300K for air; besides, saturation vapor pressure at atmospheric pressure is 373.15K. The heat flux, which varies depending on the different fluid heights, is considered close to the critical heat flux.

The overall dimensions of the chamber are considered 5.0×10×0.5 cm. In the present study, we initially predicted the heat flux interval for which the boiling is occurred in the form of nuclear boiling. Then the effect of fluid height inside the chamber on different dynamic parameters, and also the effect of natural convection on this phenomenon has been studied. The different dimensionless height of the fluid inside the chamber is defined as follows. The thermo-physical properties

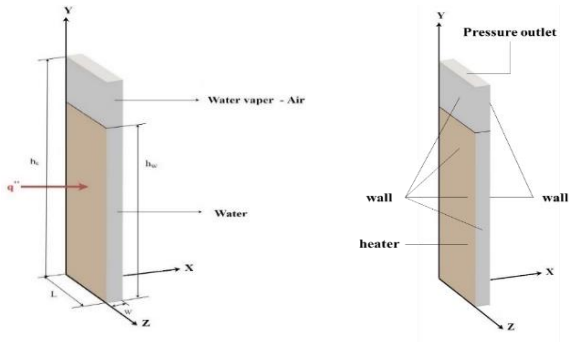

Figure 1. Schematic of the geometry and boundary conditions

used in Table 1 are listed.

$$H = \frac{h_w}{h_c} \quad (1)$$

Mesh study

In this research, Ansys meshing software was used for the meshing of the model. The grid used in this research is regular and structured. The mesh used here is shown in the Figure 2.

To choose the appropriate grid size and time step, the values of the average volume fraction of steam on the wall with a constant heat flux in t=0.1s are given in Tables 2 and 3 respectively for different grid sizes and time steps.

Table 1. Thermo-physical properties of fluids used at saturation temperature

Property	Water	Vapor	Air
ρ (kg/m^3)	958.1	0.5977	1.225
C_p(J/kg.K)	4215	2034	1006.43
k (W/m.K)	0.6775	0.0248	0.0242
μ (kg/m.s) ×10^{-4}	2.822	1.206	1.789
α (m^2/s)	1.667×10^{-7}	-	-
σ (N/m)	5.878×10^{-2}	-	-
h_{fg} (J/kg.mol)	4.0626×10^7	-	-

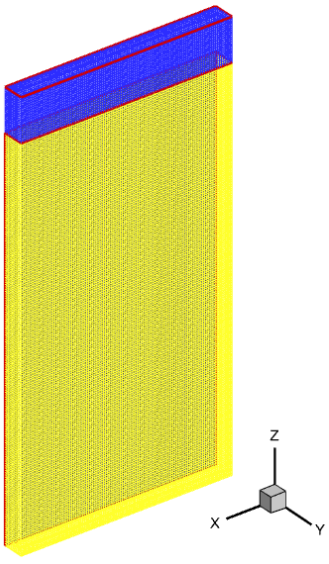

Figure 2. The grid used in this research

Table 2. Average volume fraction of steam for different network sizes

Grid size	Average volume fraction of steam on the wall with constant heat flux in t=0.1s
0.002	0.022193497
0.001	0.027814616
0.0005	0.041005254
0.00025	0.042225092

Table 3. Average volume fraction of steam for different network sizes

Grid size	Average volume fraction of steam for different time steps
0.01	0.039659206
0.001	0.039213736
0.0005	0.041005254
0.0001	0.041010268

Governing equations

In this study, two-phase fluid volume (VOF) approach was used for modeling boiling on the vertical wall and two-phase flow. In this model, considering the possibility of following two-phase contact surfaces, the model is widely used in the study of two-phase currents where phase-surface joint changes are particularly important in the welding phenomenon. The VOF model is a surface tracking technique applied to a Eulerian mesh. this model, when the interconnection of the interconnecting fluid segments is concerned, is designed to simulate two or more immiscible materials. In this model, a set of momentum equation is solved for all fluid phases and the volume fraction of each fluid in each computational cell is tracked along the solution domain. Applications of this model covers stratified flow, filling, turbulence, free surface flow, motion of large bubbles inside the fluid, fluid movement after dam failure, prediction of a jet (due to surface tension), determination of liquid-gas interface and boiling of liquids. In the VOF model, the governing equations are solved via the volume fraction in each cell. In each cell, the sum of the volume fraction of the phases is equal to one unit (Equation (2)).

$$\sum_{k=1}^{n} \alpha_k = 1 \quad (2)$$

Figure 3 shows how the volume fraction in each cell is determined. α=1 and α=0 represent the vapor and liquid phases, respectively. 0<α<1 represents the interface of two fluids [28].

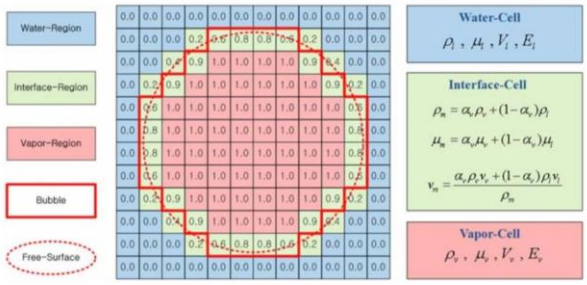

Figure 3. The volume fraction and properties per cell in the bubble simulation [28]

In the VOF model, all properties are calculated using the volume fraction of each cell. For example, in the two-phase system if the phase is specified by indices 1 and 2, and in case the volume fraction of the second phase is examined, the density in each cell is calculated as follows:

$$\rho = \alpha_2 \rho_2 + (1-\alpha_2)\rho_1 \quad (3)$$

All other properties are calculated in the same way. Thus, according to the volume fraction, the properties in each cell would be different and the governing equations would be solved based on these properties.

Continuity

In the VOF model, changes in the bubble level are predicted based on solving the continuity equation for the volume fraction. This equation is expressed as follows:
Liquid phase;

$$\frac{\partial \rho_l \alpha_l}{\partial t} + \nabla(\rho_l \alpha_l \overrightarrow{v_l}) = S_{lv} \quad (4)$$

Vapor phase;

$$\frac{\partial \rho_v \alpha_v}{\partial t} + \nabla(\rho_v \alpha_v \overrightarrow{v_v}) = S_i - f S_{lv} \quad (5)$$

In above relation S_{lv} and S_{lv} source terms are related to mass transfer. Mass transfer between phases in bubble condensation can be modeled using these terms. Also, S_i is the additional source term related to the joining and breaking up of bubbles, f is the scalar fraction related to the density of the number of discrete bubbles.

Momentum

In the VOF model, the momentum relationship is solved in the entire domain and the obtained velocity field is applied to all the existing phases. This equation for liquid and vapor phases is expressed as follows:
Liquid phase;

$$\frac{\partial \rho_l \alpha_l \overrightarrow{u_l}}{\partial t} + \nabla \cdot (\rho_l \alpha_l \overrightarrow{u_l}\overrightarrow{u_l}) = -\alpha_l \nabla \mathrm{p} + \alpha_l \rho_l \vec{g} + \nabla[\alpha_l \mu_l^e (\nabla \overrightarrow{u_l} + (\nabla \overrightarrow{u_l})^T)] + (S_{lv}\overrightarrow{u_l} - S_{vl}\overrightarrow{u_v}) + F_{lv} \quad (6)$$

Vapor phase;

$$\frac{\partial \rho_v \alpha_v \overrightarrow{u_v}}{\partial t} + \nabla \cdot (\rho_v \alpha_v \overrightarrow{u_v}\overrightarrow{u_v}) = -\alpha_v \nabla \mathrm{p} + \alpha_v \rho_v \vec{g} + \nabla[\alpha_v \mu_v^e (\nabla \overrightarrow{u_v} + (\nabla \overrightarrow{u_v})^T)] + (S_{vl}\overrightarrow{u_l} - S_{lv}\overrightarrow{u_v}) + F_{vl} \quad (7)$$

In the relationships between the terms $F_{lv}$and F_{vl}, it represents the surface tension force on the surface of the bubble and the buoyancy force, the following relationship exists between them:

$$F_{lv} = -F_{vl} \quad (8)$$

Energy

The energy equation for liquid and vapor phases is as follows:
Liquid phase;

$$\frac{\partial \rho_l \alpha_l H_l}{\partial t} + \nabla \cdot (\rho_l \alpha_l \overrightarrow{u_l} H_l) = \nabla[\alpha_l \mu_l^e (\nabla T_l)] + (S_{lv}H_l - S_{vl}H_v) \quad (9)$$

Vapor phase;

$$\frac{\partial \rho_v \alpha_v H_v}{\partial t} + \nabla \cdot (\rho_v \alpha_v \overrightarrow{u_v} H_v) = \nabla[\alpha_v \mu_v^e (\nabla T_v)] + (S_{lv}H_v - S_{vl}H_l) \quad (10)$$

In the above relations, H is enthalpy.

RESULTS AND DISCUSSION

To check the accuracy of the modeling method, the obtained heat flux values for the specified temperature difference between the wall and the fluid and the shape of the bubbles near the vertical wall have been compared with the experimental research of Kaneyasu et al. [29], it is given in Table 4 and Figure 4.

Figure 5 shows a part of the surface covered by the vapor phase near the time of the boiling point change. The minimum value is assigned to the dimensionless height equal to 0.3. The boiling regime at the dimensionless height of 0.5 enters the boiling regime earlier than the height of 0.7, so it has more bubble-covered surface than the dimensionless height of 0.7 at time t = 0.15 s. The highest value is assigned to the dimensionless height of 0.9, which is due to having a higher heat flux and

Table 4. Comparison of heat flux for specific temperature difference in the current study and experimental study of Kaneyasu et al. [29]

ΔT_{Sat}	q'' (W/m^2) Nishikawa et al [30]	q'' (W/m^2) Present study	Error (%)
5	1.5×10^4	1.7×10^4	13.34
10	7×10^4	6.7×10^4	4.28
20	4×10^5	3.6×10^5	10

generating more bubbles than the dimensionless heights. In general, with increasing dimensionless height of the fluid in the chamber and the Rayleigh number, the production of bubbles and the percentage of the surface on which the steam exists, is increased. Figures 5 to 9

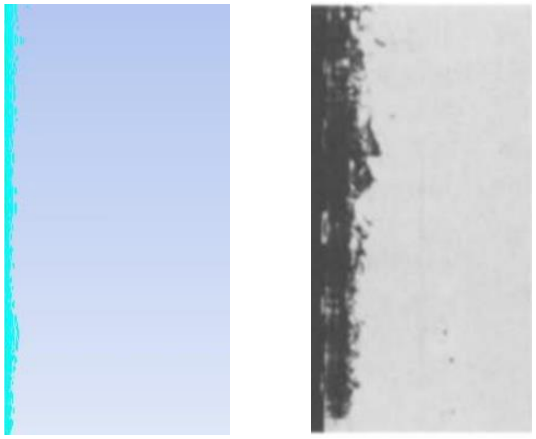

(a) (b)

Figure 4. Comparison of the shape of the bubbles near the vertical wall in the present study (a) and the experimental study of Nishikawa et al. [29] for q" = 120 kW (b)

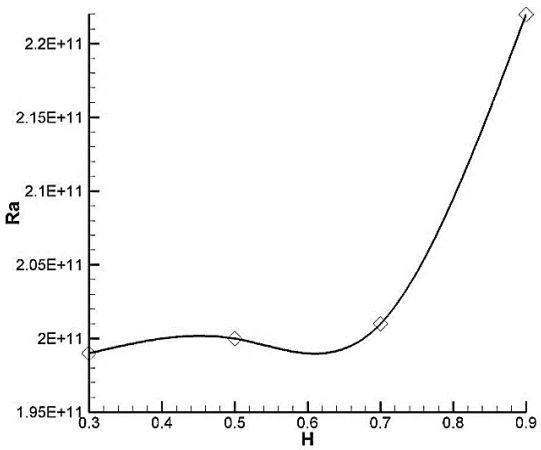

Figure 5. The percentage of surface covered with steam on hot wall (t = 0.15 s)

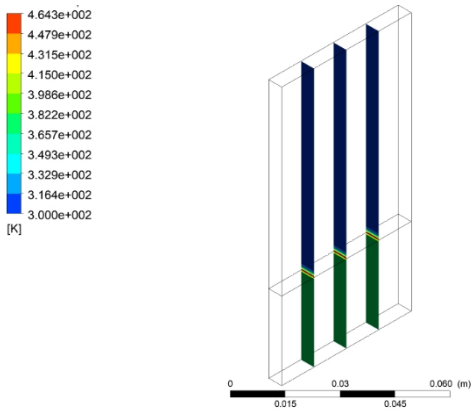

Figure 6. the temperature distribution in three dimensions at t = 0.1 S and H = 0.5

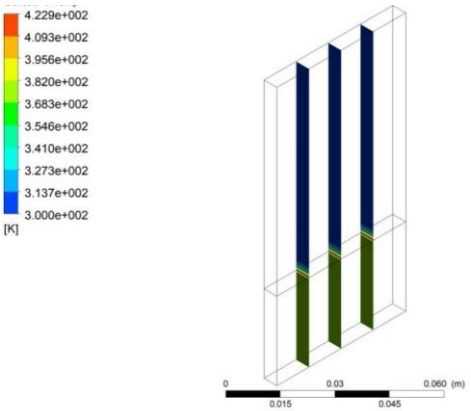

Figure 7. the temperature distribution in three dimensions at t = 0.05 S and H = 0.3

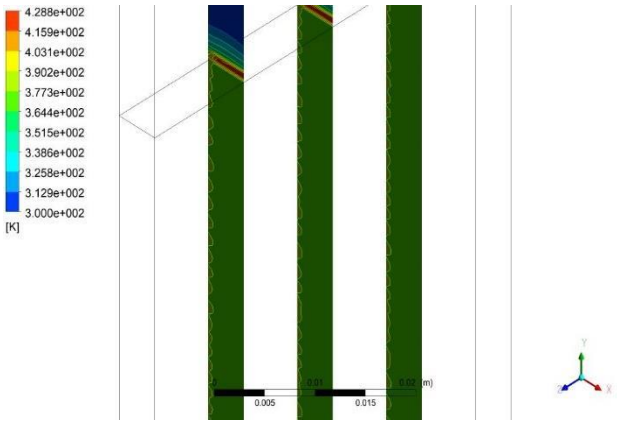

Figure 8. the temperature distribution in three dimensions at t = 0.15 S and H = 0.7

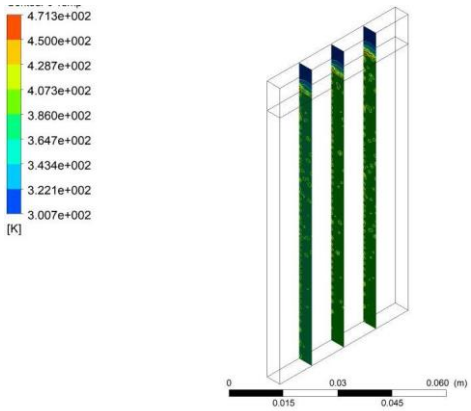

Figure 9. The temperature distribution in three dimensions at t = 0.2 S and H = 0.9

show the temperature distribution in three dimensions at different fluid times near the boiling point change. Under the equal conditions, according to the temperature contour, it can be mentioned that the general temperature of the liquid in the chamber has increased with increasing the fluid height. Also, the air temperature above the water in the tank is remained constant up to the dimensionless height of 0.7, and only for the dimensionless height of 0.9, the air temperature above the chamber has gradually increased, which is due to the existence of much steam in this area. In general, the temperature of steam and water in the chamber decreases by being far from the wall with a constant heat flux. Also, the temperature distribution of fluid dimensionless heights less than 0.9 is much uniform. For a dimensionless height of 0.9 similar to a wall with wall contours having a constant heat flux, the temperature difference between water and steam in the chamber is about 20-60 degrees Kelvin.

Figure 10 illustrates the temperature distribution on the hot wall at a time close to the change in boiling regime. For a dimensionless height of 0.3, the temperature distribution is non-uniform, and as mentioned earlier, the variation time is very short. Compared to other dimensionless heights, the maximum temperature due to the presence of more vapor volume fraction in the free surface is more considerable for the dimensionless height of 0.7. For a dimensionless height of 0.9, the temperature difference between water and steam on the wall is highly visible and is around 20 to 60 degrees Kelvin.

Figure 11 shows a diagram of temperature changes in a wall with a constant heat flux for different dimensionless heights. Dimensionless height 0.9 has a higher average temperature than other dimensionless heights due to having a higher critical heat flux. For the rest of the dimensionless heights, a relatively uniform distribution is presented in this figure. For all dimensionless heights of temperature maximum, there is a maximum temperature near the free surface, as can be seen in the temperature distribution counters, is due to the steam accumulation in this area.

Figure 12 shows a diagram of the temperature distribution along the X axis inside the chamber. The effect of the steam presence in different areas in this diagram is quite significant as for dimensionless heights less than 0.9 due to the presence of more steam phase near the wall with a higher heat flux there is a temperature only near the wall, which this distance is about 0.0005 m for dimensionless height of 0.3 and 0.5 and 0.001m for dimensionless height of 0.7. For dimensionless height of 0.9, the temperature distribution is different due to the existence of steam in different parts. The process of temperature change for this dimensionless height is decreasing to the center of the chamber and then

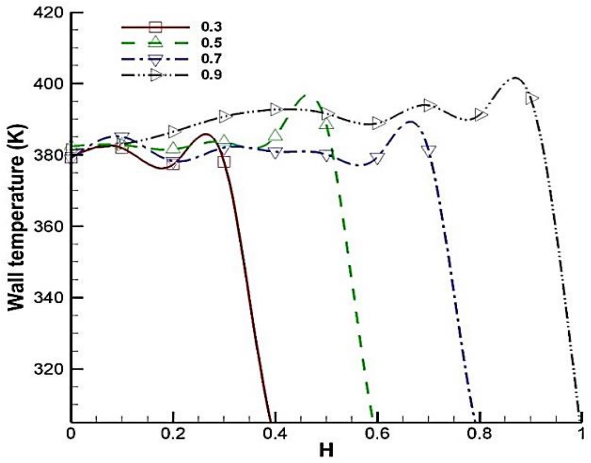

Figure 11. The temperature in a wall with a constant heat flux for different dimensionless heights

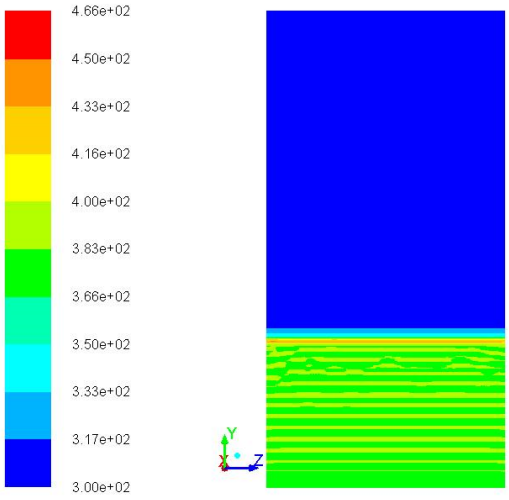

Figure 10. The temperature distribution on the hot wall at a time close to the change in boiling regime

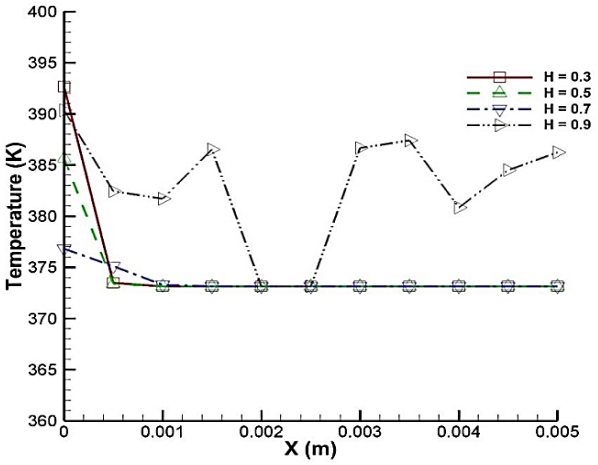

Figure 12. The temperature distribution along the X axis inside the chamber

increasing. This can have occurred under the influence of currents caused by the effect of natural convection inside the chamber and the transfer of bubbles with higher temperatures near the walls. The changes in the velocity field distribution over time for different dimensionless heights of the fluid are shown in Figures 11 to 16. According to these figures, for all dimensionless heights vortices due to natural convection are formed in the lower parts of the chamber over time, and gradually these vortices are expanded and activated in many parts of the fluid.

For dimensionless heights less than 0.9, where the presence of bubbles is limited to the area near the wall with a heat flux, with a lower Rayleigh number, the velocity field distribution is more uniform. Also, due to the presence of many bubbles formed on the wall and the impossibility of fluid infiltration into the areas with bubbles, vortices caused by natural convection are affected. However, due to the limited presence of bubbles near the wall with heat flux, the general and uniform form of vortices remain unchanged in a major part of the fluid. On the other hand, with the production of more bubbles over time, the bubbles move toward the free surface due to their lower density. Also, this phenomenon is due to the dominance of the buoyant force over the force arising from gravitational field. Along with the movement of bubbles, part of the fluid in the proximity of the bubbles is also moved by the movement of bubbles, which is faster than the movement of fluid due to natural convection, so the maximum speed exists near the wall with heat flux.

At a dimensionless height of 0.9, stronger vortices are formed due to natural convection by increasing the height of the fluid inside the chamber. Also, this dimensionless height has a higher Raleigh number as having a higher heat flux. In this case, the production of bubbles increases over time due to the continuous use of heat flux. At the beginning of the modeling time, similar vortices due to natural convection are formed uniformly at the bottom of the chamber before producing bubbles similar to dimensionless heights. However, when the first bubble departs from the uniform field surface, the natural convection is completely influence and gradually gets turbulent. Given the time t = 0.1 S, the turbulence also is started at the bottom of the chamber. Turbulence of flow fields encompasses its deformation or division of the general flow field into smaller fields with local effect in different areas, especially near the free surface.

The maximum velocity at different times inside the chamber simulation is illustrated in Figure 17. As natural convection becomes more active over time, the maximum velocity is increased. Also, the maximum speed is directly associated with the value of the Raleigh number inside the chamber, so that for dimensionless height less than 0.9, which has almost the same Raleigh values has the maximum speed values close to each other. For a dimensionless height of 0.9 that has a higher Raleigh number than lower dimensionless heights, the maximum

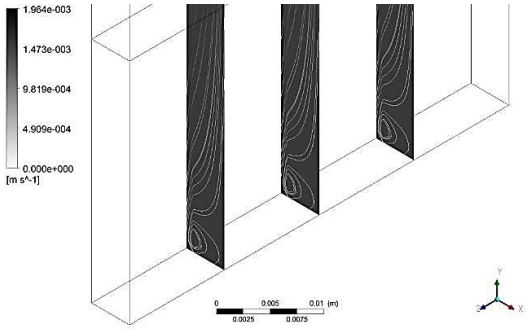

Figure 13. The velocity filed distribution at t = 0.05 S and H = 0.3

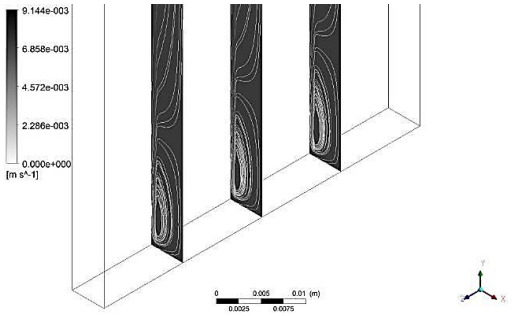

Figure 14. The velocity filed distribution at t = 0.1 S and H = 0.5

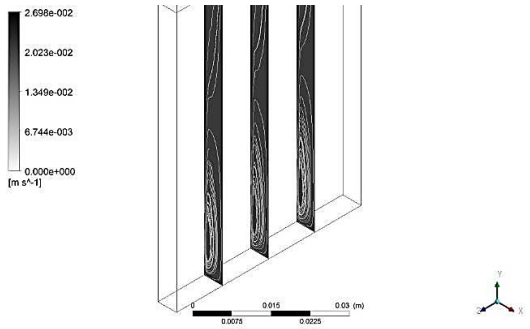

Figure 15. The velocity filed distribution at t = 0.15 S and H = 0.7

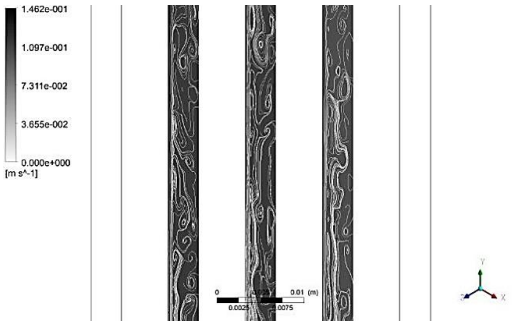

Figure 16. The velocity filed distribution at t = 0.2 S and H = 0.9

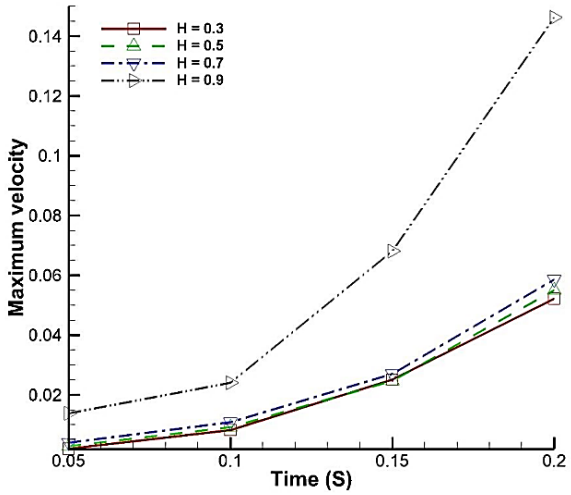

Figure 17. The maximum velocity at different times inside the chamber

velocity changes are higher over time. This phenomenon can be due to the increased turbulence made by the bubbles presence in different parts of the chamber and the fluid movement by the bubbles.

The distribution of the volume fraction for vapor, or the bubble production sites, is depicted in Figures 18 to 21 on a wall with a constant heat flux in the direction of the Y and Z axes. Due to the nature of the boiling phenomenon, the distribution of bubble production sites is non-uniform, so that for different dimensionless heights, the location of active bubble production sites is different. In general, more active sites are located near the free surface due to the higher surface temperature. For dimensionless heights of 0.9, which has the highest bubble production, unlike less dimensionless heights, more active sites are far from the free surface of the fluid. Active sites along the Z axis are located at dimensionless heights less than 0.5 in the second half and at

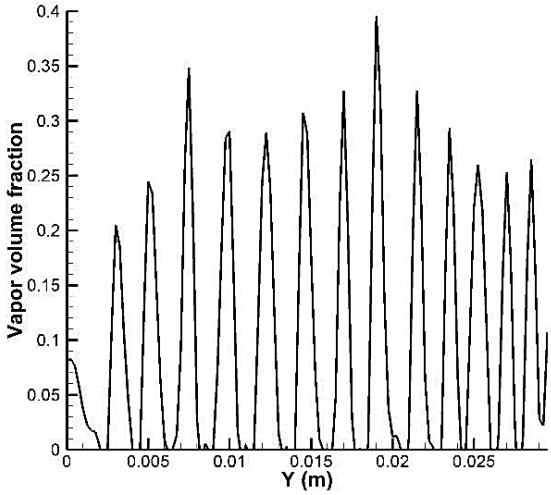

Figure 18. The distribution of the volume fraction for vapor at H = 0.3

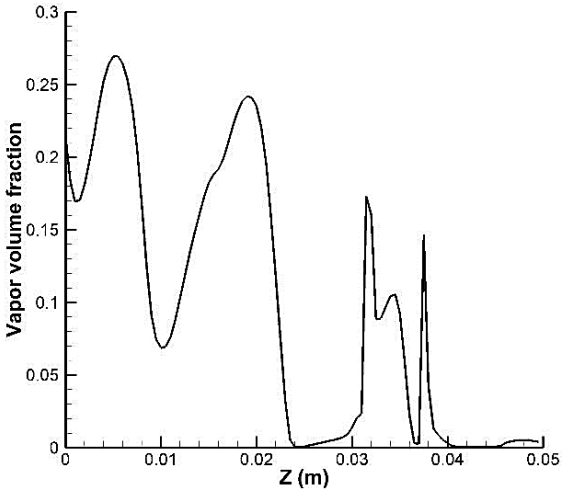

Figure 20. The distribution of the volume fraction for vapor at H = 0.7

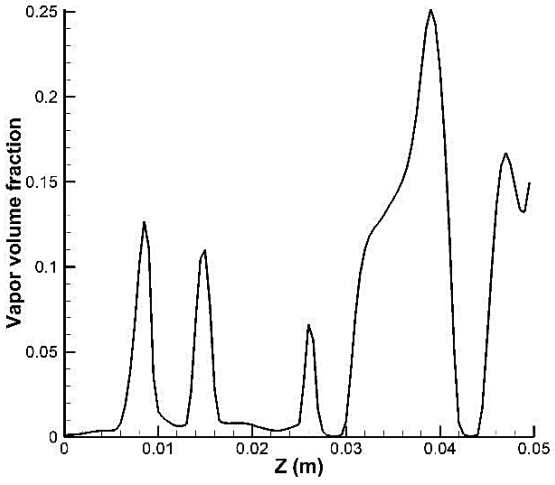

Figure 19. The distribution of the volume fraction for vapor at H = 0.5

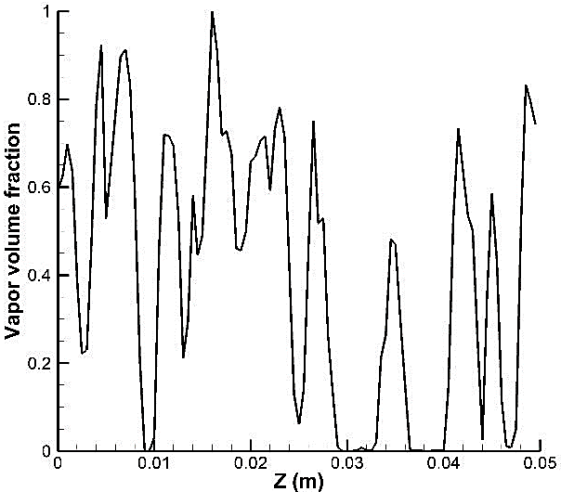

Figure 21. The distribution of the volume fraction for vapor at H = 0.9

dimensionless heights greater than 0.5 in the first half. It is worth to mention that for dimensionless heights less than 0.9, the volume fraction of steam has low values.

The diagram of changes in the volume fraction for steam with a time up to 0.2 s for different dimensionless heights of water is illustrated in Figure 22. For dimensionless heights less than 0.9, which enter the film boiling regime in less than 0.2 seconds, in the change from boiling regime to average film, the average volume fraction for steam is increased, this phenomenon for dimensionless height 0.3 is more obvious. For a dimensionless height of 0.9, which is always nucleate boiling regime to the end of the study period, the maximum volume fraction is almost constant during bubble production periods.

Figure 23 shows the average growing period of the bubble, and the reactivation of the bubble production sites (waiting period) for different dimensionless heights of water. Due to the bubble forms for different heights, the dimensionless heights of 0.9 where nucleate boiling as the dominant regime have been reduced by an average of 50% compared to the lower heights of the average growth time. At lower dimensionless heights, with higher bubble growth time, the bubbles connect faster after full growth, so the dominant boiling regime quickly changes to the film boiling regime. Similar to bubble growth time, the time required to reactivate bubble production sites for a dimensionless height of 0.9, which has the highest bubble production, is much shorter than for other dimensionless heights. Dimensional height 0.5 has the longest reactivation time of bubble production sites. Also, as mentioned in experimental research [30], approximately, the average time required to reactivate bubble production sites is three times the average bubble growth time ($t_w = 3t_g$).

In the present study, by increasing the height of the fluid inside the chamber, the constant heat flux on the wall has ascending trend, so for higher dimensionless fluid heights, over time, the difference between wall and fluid temperature, or the degree of superheat of the wall is increased. In the study of Han and Griffith [31], a decreasing trend for the reactivation time of bubble production sites with increasing degree of wall superheat is predicted, which in the present study, a similar trend is observed in Figure 23. Also, similar to the time of reactivation of bubble production sites, Zuber [32], showed a decreasing trend for the average bubble growth time in his study, which can be seen for the average bubble growth time in the present study in Figure 23.

Figure 24 shows the bubble production frequency for different dimensionless heights of the fluid. The frequency of bubble production has an ascending trend with increasing dimensionless height of the fluid inside the chamber. Also, in general, the frequency of bubble production is inversely related to the total average time required to reactivate bubble production sites and the bubble growth period. Peebles and Garber have presented an equation as follows to predict the frequency of bubble production, which is compared with the results of the present study with the mentioned equation in Figure 24.

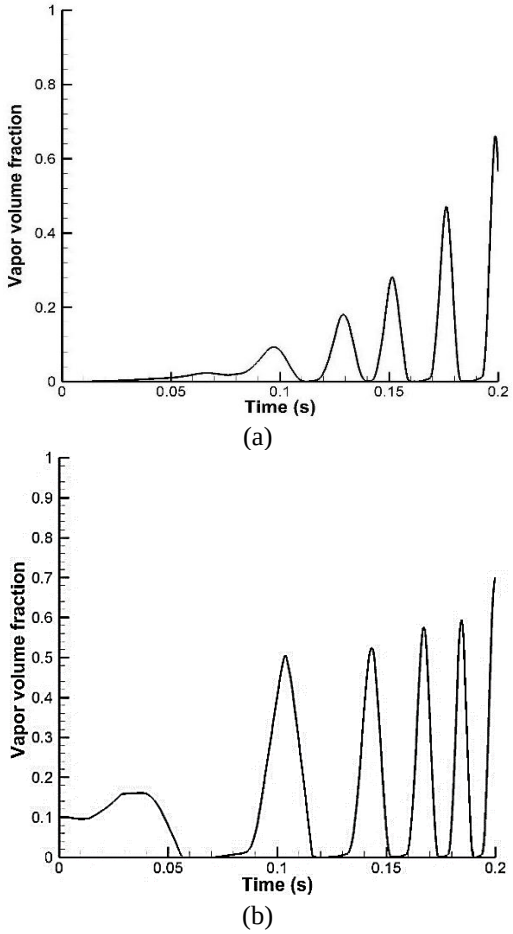

Figure 22. the volume fraction for steam with a time up to 0.2 s for different dimensionless heights, H = 0.5 (a) and 0.9 (b)

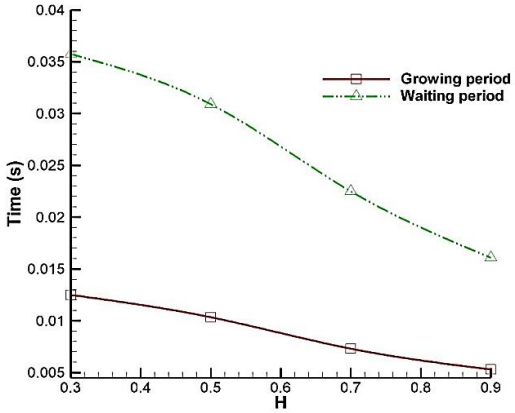

Figure 23. The average growing period of the bubble and the reactivation of the bubble production sites

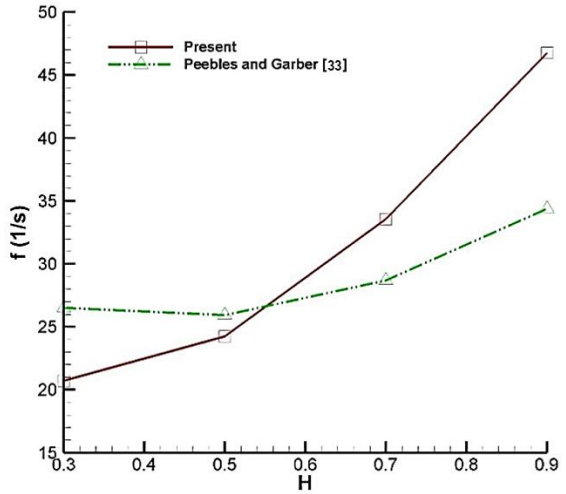

Figure 24. the bubble production frequency for different dimensionless heights of the fluid [33]

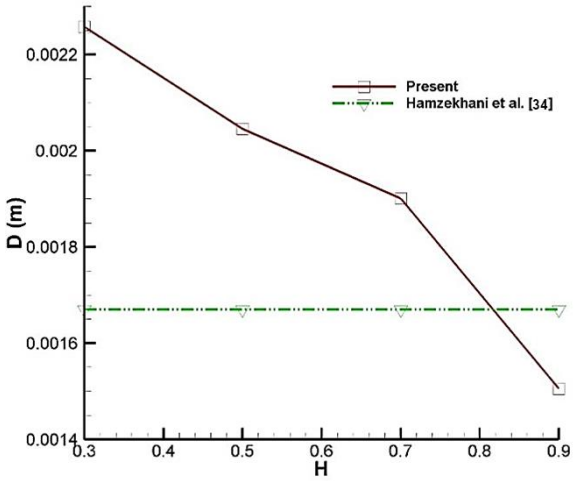

Figure 26. The average bubble diameter for different dimensionless heights [34]

In the present study, plot digitizer software was used to measure the bubble diameter. In this software, as shown in Figure 25 as an example for a dimensionless height of 0.9, after calibrating the contours of volume fraction of steam, the diameter of several bubbles has been measured. The average measurements performed for different dimensionless heights of the fluid are given as follows:

The average bubble diameter for different dimensionless heights in departure from the surface with heat flux is shown in Figure 26. According to the measurement of bubble diameter in the nucleate boiling regime, the bubbles have a small diameter, about 0.002 m.

Hamzekhani et al. [34] presented a relation as follows to predict the diameter of the bubble. The comparison of the results of the present study with the mentioned relation is also depicted in Figure 22.

In this paper, to obtain a coefficient of heat transfer with specific heat flux on the wall, the temperature on the wall and the fluid temperature in the proximity of the wall as a set of points, the output is taken from the Fluent software and is based on the height of the chamber of curve fit ((T = f (y)) and finally the heat flux is divided by

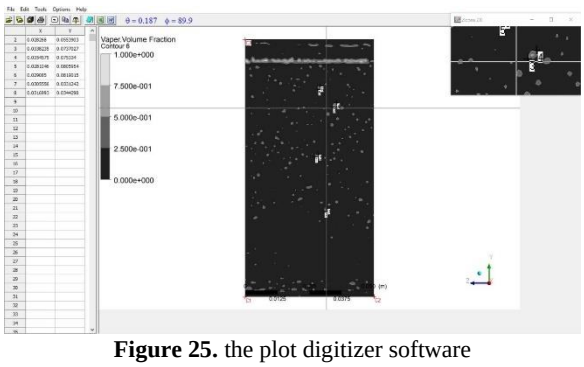

Figure 25. the plot digitizer software

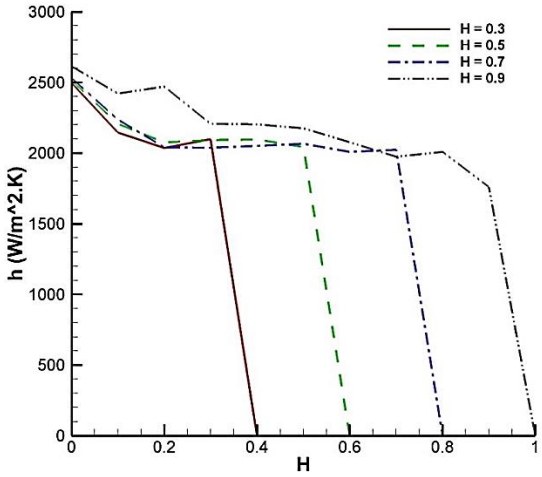

Figure 27. The displacement heat transfer coefficient

the temperature difference and the heat transfer coefficient is calculated.

Figure 27 shows the displacement heat transfer coefficient for different dimensionless heights at different periods close to the boiling regime change. At the dimensionless height of 0.9, due to the dominance of the nucleate boiling regime and the production of bubbles at a higher speed compared to other dimensionless heights, it is possible to transfer more heat from the surface. Other dimensionless heights less than 0.9 have almost the same behavior in this respect.

The changes in displacement heat transfer coefficient over time are illustrated in Figure 28. In the early stages of simulation and before the production of bubbles, the heat transfer coefficient at different dimensional heights has a small value and for dimensionless heights less than 0.9 has almost the same value. With the formation of nucleate boiling over time, this amount increases significantly, and then tends to be almost constant.

Dimensional height 0.9 has a higher heat transfer coefficient than other dimensionless heights due to having a higher critical heat flux and keeping the nucleate boiling regime at longer times than other dimensionless heights. Dimensional heights less than 0.9 have a relatively similar behavior over time. Also, when natural convection is the dominant heat transfer regime and bubbles from nuclear boiling have not yet been formed, the heat transfer coefficient does not change considerably over time.

The effect of Rayleigh number changes on the heat transfer coefficient is shown in Figure 29. As the Rayleigh number is increased, the vortex power arising from the natural convection inside the chamber is increased. This phenomenon directly influences the rate of heat transfer and improves it. Also, more active currents due to natural fluid convection is an important factor and accelerates the departure of bubbles and fluid movement. On the other hand, with the increase of Rayleigh number and the presence of more bubbles in different areas of the chamber, the flow gets non-uniform and turbulent, which significantly improves the amount of heat transfer.

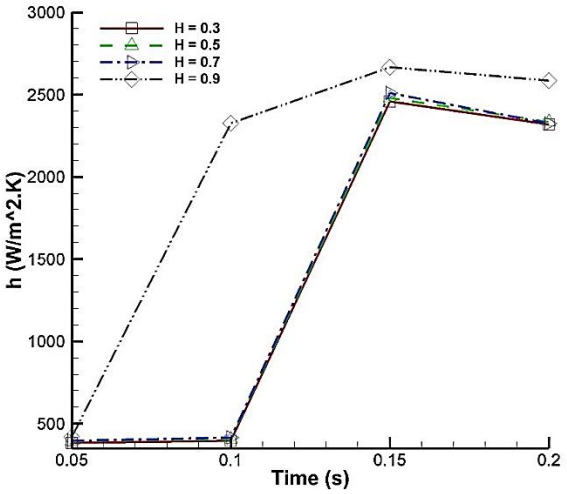

Figure 28. heat transfer coefficient by time

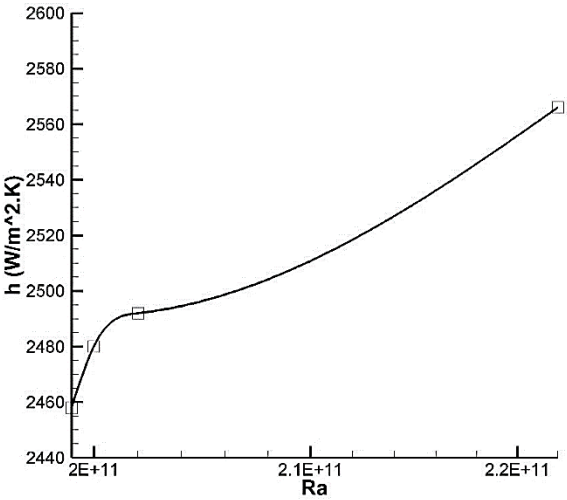

Figure 29. The effect of Rayleigh number changes on the heat transfer coefficient

By examining the various experimental relations presented to express the heat transfer coefficient in the bubble dynamic parameters affecting it, it can be said that the bubble diameter is one of the effective dynamic properties [35-40]. However, there is no experimental research exactly similar to the present study, this comparison is made in general given below.

Jung et al. [41] presented a relation for predicting the heat transfer coefficient for nucleate boiling. This equation is based on the thermo-physical properties, heat flux and bubble diameter as mentioned. Figure 30 shows the changes in the heat transfer coefficient with the changes in the bubble diameter. As shown in the curve fit shown in the figure, the changes in the heat transfer coefficient are an exponential function of the bubble diameter. A comparison of the relationship between the curve fit of the present study and the present study is given in Table 5. This comparison indicates the same behavior of the heat transfer coefficient with the bubble diameter.

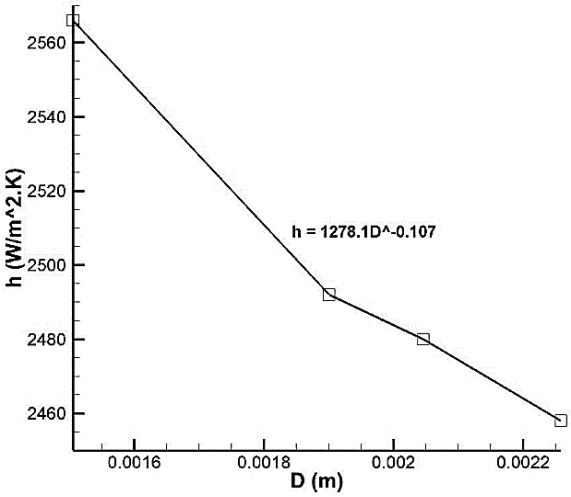

Figure 30. The heat transfer coefficient with the changes in the bubble diameter

Table 5. The heat transfer coefficient formulation

Jung et al. [41]	Present
$h = C\ D^{-0.08}$	$h = 1278.1\ D^{-0.107}$

CONCLUSION

In the present study, a chamber having immiscible fluids, water, steam and air, and also a side wall with uniform

heat flux was studied in 3D. Here, the numerical study of boiling from the vertical wall of a chamber with different fluid heights and the effect of natural convection on this phenomenon is discussed, the results of which are as follows:

It should be noted that the distribution of the velocity field follows more uniform pattern in dimensionless heights less than 0.9. In this case, bubbles are only present near a wall with heat flux that has a lower Rayleigh number. Also, existence of these bubbles on the wall, which prevents fluid infiltration into this area, affects vortices caused by natural convection. However, the general and uniform patterns of vortices remain unchanged in most part of the fluid, which is because of the limited amount of bubbles near the wall with heat flux.

Natural convection increases the height of fluid inside the chamber, which leads to the formation of strong vortices at a dimensionless height of 0.9 that has a higher Raleigh number because of a higher heat flux. In this case, the continuous use of heat flux gives rise to the production of bubbles over time.

According to the present study, suggestions for future studies can be as follows:

- The use of different turbulence models to investigate the flow shape and the amount of heat transfer due to the relatively turbulent shape of the flow.
- Investigating the effect of placing the chamber at an angle to the horizontal to study the effect of gravity.
- Investigating the effect of adding electrolyte or nanofluid to the chamber on the heat transfer rate.

REFERENCES

1. Jakob, M., 1949. Heat Transfer, John Wiley & Sons, New York.
2. Hsu, Y.-Y. and Graham, R. W., 1976. Transport processes in boiling and two-phase systems, including near-critical fluids, *Washington*.
3. Lee, R. and Nydahl, J., 1989. Numerical calculation of bubble growth in nucleate boiling from inception through departure, *ASME Journal of Heat Transfer*, 111(2), pp. 474–479. Doi:10.1115/1.3250701
4. Welch, S. W., 1998. Direct simulation of vapor bubble growth, *International Journal of Heat and Mass Transfer*, 41(12), pp. 1655-1666. Doi:10.1016/S0017-9310(97)00285-8
5. Lay, J. and Dhir, V., 1995. Shape of a vapor stem during nucleate boiling of saturated liquids, *ASME Journal of Heat Transfer*, 117(2), pp. 394–401. Doi:10.1115/1.2822535
6. Son, G., Dhir, V. K. and Ramanujapu, N., 1999. Dynamics and heat transfer associated with a single bubble during nucleate boiling on a horizontal surface, *ASME Journal of Heat Transfer*, 121(3), pp. 623–631. Doi:10.1115/1.2826025
7. Son, G., Ramanujapu, N. and Dhir, V. K., 2002. Numerical simulation of bubble merger process on a single nucleation site during pool nucleate boiling, *ASME Journal of Heat Transfer*, 124(1), pp. 51-62. Doi:10.1115/1.1420713
8. Mukherjee, A. and Dhir, V., 2004. Study of lateral merger of vapor bubbles during nucleate pool boiling, *ASME Journal of Heat Transfer*, 126(6), pp. 1023-1039. Doi:10.1115/1.1834614
9. Shin, S., Abdel-Khalik, S. and Juric, D., 2005. Direct three-dimensional numerical simulation of nucleate boiling using the level contour reconstruction method, *International Journal of Multiphase Flow*, 31(10-11), pp. 1231-1242. Doi:10.1016/j.ijmultiphaseflow.2005.06.005
10. Yoon, H. Y., Koshizuka, S. and Oka, Y., 2001. Direct calculation of bubble growth, departure, and rise in nucleate pool boiling, *International Journal of Multiphase Flow*, 27(2), pp. 277-298. Doi:10.1016/S0301-9322(00)00023-9
11. Son, G. and Dhir, V. K., 2008. Numerical simulation of nucleate boiling on a horizontal surface at high heat fluxes, *International Journal of heat and Mass transfer*, 51(9-10), pp. 2566-2582. Doi:10.1016/j.ijheatmasstransfer.2007.07.046
12. Chu, H. and Yu, B., 2009. A new comprehensive model for nucleate pool boiling heat transfer of pure liquid at low to high heat fluxes including CHF, *International Journal of Heat and Mass Transfer*, 52(19-20), pp. 4203-4210. Doi:10.1016/j.ijheatmasstransfer.2009.04.010
13. McHale, J. P. and Garimella, S. V., 2013. Nucleate boiling from smooth and rough surfaces–Part 2: Analysis of surface roughness effects on nucleate boiling, *Experimental Thermal and Fluid Science*, 44, pp. 439-455. Doi:10.1016/j.expthermflusci.2012.08.005
14. Hutter, C., Sanna, A., Karayiannis, T., Kenning, D., Nelson, R., Sefiane, K. and Walton, A., 2013. Vertical coalescence during nucleate boiling from a single artificial cavity, *Experimental Thermal and Fluid Science*, 51, pp. 94-102. Doi:10.1016/j.expthermflusci.2013.07.005
15. Sanna, A., Hutter, C., Kenning, D., Karayiannis, T., Sefiane, K. and Nelson, R., 2014. Numerical investigation of nucleate boiling heat transfer on thin substrates, *International Journal of Heat and Mass Transfer*, 76, pp. 45-64. Doi:10.1016/j.ijheatmasstransfer.2014.04.026
16. Jung, S. and Kim, H., 2014. An experimental method to simultaneously measure the dynamics and heat transfer associated with a single bubble during nucleate boiling on a horizontal surface, *International Journal of Heat and Mass Transfer*, 73, pp. 365-375. Doi:10.1016/j.ijheatmasstransfer.2014.02.014
17. Kunkelmann, C. and Stephan, P., 2010. Numerical simulation of the transient heat transfer during nucleate boiling of refrigerant HFE-7100, *International Journal of Refrigeration*, 33(7), pp. 1221-1228. Doi:10.1016/j.ijrefrig.2010.07.013
18. Jia, H., Zhang, P., Fu, X. and Jiang, S., 2015. A numerical investigation of nucleate boiling at a constant surface temperature, *Applied Thermal Engineering*, 88, pp. 248-257. Doi:10.1016/j.applthermaleng.2014.09.022
19. Ling, K., Li, Z.-Y. and Tao, W.-Q., 2014. A Direct Numerical Simulation for Nucleate Boiling by the VOSET Method, *Numerical Heat Transfer, Part A: Applications*, 65(10), pp. 949-971. Doi:10.1080/10407782.2013.850971
20. Lal, S., Sato, Y. and Niceno, B., 2015. Direct numerical simulation of bubble dynamics in subcooled and near-saturated convective nucleate boiling, *International Journal of Heat and Fluid Flow*, 51, pp. 16-28. Doi:10.1016/j.ijheatfluidflow.2014.10.018
21. Utaka, Y., Kashiwabara, Y. and Ozaki, M., 2013. Microlayer structure in nucleate boiling of water and ethanol at atmospheric pressure, *International Journal of Heat and Mass Transfer*, 57(1), pp. 222-230. Doi:10.1016/j.ijheatmasstransfer.2012.10.031
22. Marcus, B. and Dropkin, D., 1963. The effect of surface configuration on nucleate boiling heat transfer, *International Journal of Heat and Mass Transfer*, 6(9), pp. 863-866. Doi:10.1016/0017-9310(63)90069-3
23. Sarker, D., Franz, R., Ding, W. and Hampel, U., 2017. Single bubble dynamics during subcooled nucleate boiling on a vertical heater surface: An experimental analysis of the effects of surface

characteristics, *International Journal of Heat and Mass Transfer*, 109, pp. 907-921. Doi:10.1016/j.ijheatmasstransfer.2017.02.017

24. Salari, M., Kasaeipoor, A. and Malekshah, E. H., 2018. Influence of static bubbles at the surface of electrodes on the natural convection flow for application in high performance lead-acid battery, *Thermal Science and Engineering Progress*, 5, pp. 204-212. Doi:10.1016/j.tsep.2017.12.001
25. Yao, S., Huang, T., Zhao, K., Zeng, J. and Wang, S., 2019. Simulation of flow boiling of nanofluid in tube based on lattice Boltzmann model, *Thermal Science*, 23(1), pp. 159-168. Doi:10.2298/TSCI160817006Y
26. Stojanović, A. D., Stevanović, V. D., Petrović, M. M. and Zivkovic, D. S., 2016. Numerical investigation of nucleate pool boiling heat transfer, *Thermal Science*, 20, pp. S1301-S1312. Doi:10.2298/TSCI160404276S
27. Kamel, M. S. and Lezsovits, F., 2019. Boiling heat transfer of nanofluids: A review of recent studies, *Thermal Science*, 23(1), pp. 109-124. Doi:10.2298/TSCI170419216K
28. Jeon, S.-S., Kim, S.-J. and Park, G.-C., Year.CFD simulation of condensing vapor bubble using VOF model, Proceedings of World Academy of Science, Engineeri ng and Technology: Citeseer, pp. 209-215. Available at: https://citeseerx.ist.psu.edu/viewdoc/download?doi=10.1.1.193.2163&rep=rep1&type=pdf
29. Kaneyasu, N., Yasunobu, F., Satoru, U. and Haruhiko, O., 1984. Effect of surface configuration on nucleate boiling heat transfer, *International Journal of Heat and Mass Transfer*, 27(9), pp. 1559-1571. Doi:10.1016/0017-9310(84)90268-0
30. Van Stralen, S., Sohal, M., Cole, R. and Sluyter, W., 1975. Bubble growth rates in pure and binary systems: combined effect of relaxation and evaporation microlayers, *International Journal of Heat and Mass Transfer*, 18(3), pp. 453-467. Doi:10.1016/0017-9310(75)90033-2
31. Chi-Yeh, H. and Griffith, P., 1965. The mechanism of heat transfer in nucleate pool boiling—Part II: The heat flux-temperature difference relation, *International Journal of Heat and Mass Transfer*, 8(6), pp. 905-914. Doi:10.1016/0017-9310(65)90074-8
32. Zuber, N., 1961. The dynamics of vapor bubbles in nonuniform temperature fields, *International Journal of Heat and Mass Transfer*, 2(1-2), pp. 83-98. Doi:10.1016/0017-9310(61)90016-3
33. Peebles FN and HJ, G., 1953. Study on motion of gas bubbles in liquids, *Chemical Engineering Progress*, 49, pp. 88–97.
34. Hamzekhani, S., Falahieh, M. M. and Akbari, A., 2014. Bubble departure diameter in nucleate pool boiling at saturation: Pure liquids and binary mixtures, *International journal of refrigeration*, 46, pp. 50-58. Doi:10.1016/j.ijrefrig.2014.07.003
35. Etbaeitabari, A., Barakat, M., Imani, A., Domairry, G. and Jalili, P., 2013. An analytical heat transfer assessment and modeling in a natural convection between two infinite vertical parallel flat plates, *Journal of Molecular Liquids*, 188, pp. 252-257. Doi:10.1016/j.molliq.2013.09.010
36. Jalili, B., Jalili, P., Sadighi, S. and Ganji, D. D., 2021. Effect of magnetic and boundary parameters on flow characteristics analysis of micropolar ferrofluid through the shrinking sheet with effective thermal conductivity, *Chinese Journal of Physics*, 71, pp. 136-150. Doi:10.1016/j.cjph.2020.02.034
37. Jalili, B., Sadighi, S., Jalili, P. and Ganji, D. D., 2019. Characteristics of ferrofluid flow over a stretching sheet with suction and injection, *Case Studies in Thermal Engineering*, 14, pp. 100470. Doi:10.1016/j.csite.2019.100470
38. Jalili, P., Ganji, D. D., Jalili, B. and Ganji, D. R. M., 2012. Evaluation of electro-osmotic flow in a nanochannel via semi-analytical method, *Thermal Science*, 16(5), pp. 1297-1302. Available at: http://www.doiserbia.nb.rs/img/doi/0354-9836/2012/0354-98361205297J.pdf
39. Jalili, P., Jalili, B., Shateri, A. and Ganji, D. D., 2022. A novel analytical approach to micropolar nanofluid thermal analysis in the presence of thermophoresis, brownian motion, and hall currents, *Case Studies in Thermal Engineering*, 35, pp. 102086. Doi:10.1016/j.csite.2022.102086
40. Mohanty, R. L. and Das, M. K., 2017. A critical review on bubble dynamics parameters influencing boiling heat transfer, *Renewable and Sustainable Energy Reviews*, 78, pp. 466-494. Doi:10.1016/j.rser.2017.04.092
41. Jung, D., Kim, Y., Ko, Y. and Song, K., 2003. Nucleate boiling heat transfer coefficients of pure halogenated refrigerants, *International Journal of Refrigeration*, 26(2), pp. 240-248. Doi:10.1016/S0140-7007(02)00040-3

Persian Abstract

چکیده

پدیده جوش هسته‌ای همیشه برای انتقال حرارت بین رژیم‌های مختلف جوش مناسب تشخیص داده شده است. مطالعه جوش به عنوان پدیده‌ای جدید در نظر گرفته می‌شود که نیازهای مختلف تحقیقاتی و صنعتی مانند انتقال حرارت در راکتورهای هسته‌ای، واحدهای خنک‌کننده، موتورهای موشکی، خنک‌کننده تجهیزات الکترونیکی، باتری‌ها و غیره را برآورده می‌کند. بخار و هوا با داشتن حاشیه جانبی با شار حرارتی یکنواخت به صورت سه بعدی مورد مطالعه قرار گرفته است. برای انجام این کار، ابتدا پیش‌بینی فاصله شار حرارتی در نظر گرفته شد که برای آن، جوش به شکل جوش هسته‌ای اتفاق می‌افتد. در این مطالعه از رویکرد حجم سیال دو فازی (VOF) برای مدل‌سازی جوش بر روی دیوار عمودی و جریان دو فاز استفاده شد. در این تحقیق از بسته نرم افزاری Ansys برای مدل‌سازی عددی و شبیه‌سازی عددی استفاده شده است. توزیع میدان سرعت از الگوی یکنواخت‌تری در ارتفاعات بدون بعد کمتر از ۰/۹ پیروی می‌کند. در این مطالعه حباب‌ها فقط در نزدیکی دیواری با شار حرارتی وجود دارند که عدد رالی کمتری دارد. همچنین وجود حباب‌ها روی دیواره که از نفوذ سیال جلوگیری می‌کند بر گردابه‌های ناشی از همرفت طبیعی تأثیر می‌گذارد. با این حال، الگوهای کلی و یکنواخت گردابه‌ها در بیشتر قسمت‌های سیال بدون تغییر باقی می‌مانند که به دلیل وجود مقدار محدود حباب در نزدیکی دیوار با شار حرارتی است. همرفت طبیعی باعث افزایش ارتفاع سیال در داخل محفظه می‌شود که منجر به تشکیل گردابه‌های قوی‌تری در ارتفاع بدون بعد ۰/۹ می‌شود که علت آن شار حرارتی زیاد با عدد رالی بالا است. در این حالت استفاده مداوم از شار حرارتی باعث تولید حباب در طول زمان خواهد شد.